C. R. Mecanique 343 (2015) 192–198

Contents lists available at ScienceDirect

Comptes Rendus Mecanique

www.sciencedirect.com

Edge cracking due to a compressive residual stress in ceramic laminates

Dominique Leguillon [a,*], Oldrich Sevecek [b], Éric Martin [c], Raul Bermejo [d]

[a] Institut Jean-le-Rond-d'Alembert, CNRS UMR 7190, Sorbonne Universités, UPMC Université Paris-6, 75005 Paris, France
[b] Institute of Solid Mechanics, Mechatronics and Biomechanics, Faculty of Mechanical Engineering, Brno University of Technology, 616 69 Brno, Czech Republic
[c] Laboratoire des composites thermo-structuraux, CNRS UMR 5801, Université de Bordeaux, 33600 Pessac, France
[d] Institut für Struktur und Funktionskeramik, Montanuniversität Leoben, A-8700 Leoben, Austria

ARTICLE INFO

Article history:
Received 23 July 2014
Accepted 6 November 2014
Available online 24 November 2014

Keywords:
Ceramic laminates
Residual stresses
Fracture mechanics
Coupled criterion

ABSTRACT

The onset of an edge crack in compressive layers of a ceramic laminate undergoing residual stresses is predicted using the stress–energy coupled criterion based on the data of the tensile strength and the toughness of the material under consideration. The proposed criterion does not contain any adjustable parameter, which is its indisputable advantage. The results of predictions of the edge crack nucleation are in a very good agreement with the experimental observations of this phenomenon. They allow us to recover and even to improve slightly an approximate formula to estimate the critical layer thickness as a function of the compressive residual stress that was proposed some years ago.

1. Introduction

Ceramics are brittle materials and several attempts to improve their apparent toughness have been made [1]. The most common approach is to fabricate laminates to promote crack deflection in order to delay the final ruin of the structure. This can be achieved by using weak interfaces including layers of pyrocarbon, for instance [2–4]. Another approach consists in adding thin interphases of a porous ceramic between the dense layers [5–7]. More recently, the idea was to create strong compressive residual stresses in some intermediate layers in order to trap the growing cracks in the compressive layers [8–11]. This latter method seems most effective, but the onset of an edge crack is observed, under some conditions, in the layers undergoing a strong compressive residual stress [8–12].

To predict the onset of such an edge crack, the coupled criterion [13,14] allows getting rid of any assumption on the existence of flaws able to trigger cracking [12]. There is no adjustable parameter in the coupled criterion, whereas in the other case the flaw size is selected so as to fit with the experimental measures. This choice is somewhat arbitrary, because it does not rely on micrographic observations. Moreover, the flaw approach analyzes the early stage of the edge cracking and assumes a further crack growth in depth and along the specimen faces (channeling) to reach the observable state, while with the coupled criterion we make the assumption that the crack appears almost simultaneously all around the specimen and then grows in depth.

* Corresponding author.
E-mail address: dominique.leguillon@upmc.fr (D. Leguillon).

http://dx.doi.org/10.1016/j.crme.2014.11.001
1631-0721/

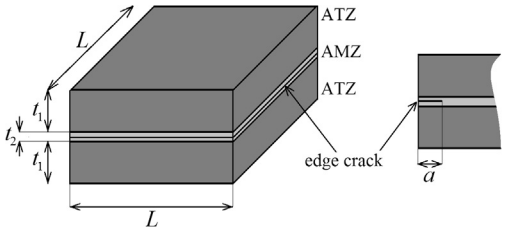

Fig. 1. The simplified 3-layer laminate and a schematic view of the edge crack with depth a in a cross section of the sample.

Table 1
Material data. E: Young's modulus, ν: Poisson's ratio, α: coefficient of thermal expansion, σ_c: tensile strength, K_{Ic}: material toughness.

Material	E (GPa)	ν	$\alpha \times 10^6$ (K^{-1})	σ_c (MPa)	K_{Ic} (MPa mm$^{1/2}$)
ATZ (1)	390	0.22	9.8	422	101.2
AMZ (2)	280	0.22	8.0	90	82.2

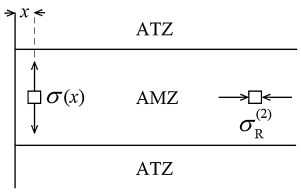

Fig. 2. The compressive residual in-plane stress $\sigma_R^{(2)}$ far from the free surface and the out-of-plane tension $\sigma(x)$ near the free surface in the AMZ layer.

2. The model

We consider a simplified symmetric ceramic laminate made of two outer layers of ATZ (thickness t_1) and one inner layer of AMZ (thickness t_2) with an edge crack of depth a running all around the specimen in the middle of the AMZ layer (Fig. 1). ATZ and AMZ are two different kinds of alumina-toughened zirconia, their elastic and fracture parameters are those given in [15] (Table 1).

The specimen length and width are $L = 4$ mm, the total thickness is $2t_1 + t_2$. The thicknesses t_1 and t_2 vary respectively from 0.4 mm to 1.5 mm and from 0.04 mm to 0.15 mm, so that the ratio $2t_1/t_2$ remains constant and equal to 20. As a consequence, for a given change of temperature $\Delta\theta$ during cooling, the layers are subjected to an in-plane bi-axial state of stress that remains unchanged for the various thicknesses [10,15], with:

$$\begin{cases} \sigma_R^{(1)} = E^{(1)*}\dfrac{(\alpha^{(2)}-\alpha^{(1)})\Delta\theta}{\frac{E^{(1)*}}{E^{(2)*}}\frac{2t_1}{t_2}+1} \\ \sigma_R^{(2)} = -E^{(2)*}\dfrac{(\alpha^{(2)}-\alpha^{(1)})\Delta\theta}{\frac{E^{(2)*}}{E^{(1)*}}\frac{t_2}{2t_1}+1} \quad \text{with } E^{(i)*} = \dfrac{E^{(i)}}{1-\nu^{(i)}} \text{ for } i=1,2 \end{cases} \tag{1}$$

For $\Delta\theta = -1000$ K, this gives $\sigma_R^{(1)} = 31.2$ MPa and $\sigma_R^{(2)} = -624$ MPa, where the upper index denotes the material: (1) for ATZ and (2) for AMZ as in Table 1.

Due to its small thickness, the AMZ layer undergoes a high compressive residual stress. Near the free edge, the stress distribution is perturbed and exhibits a strongly localized out-of-plane tensile component (Fig. 2), of the same order of magnitude as $|\sigma_R^{(2)}|$ [12], which can trigger cracking.

FE calculations are carried out in a quarter of the cross section (because of symmetries) under the assumption of plane strain. For this geometry, it is a reasonable assumption compared to full 3D calculations [16]. For each pair of thicknesses, the crack length a is varied from 0 to 0.5 mm by unbuttoning nodes. The change in potential energy $\delta W^P(a)$ between the cracked and uncracked states is computed as a function of the crack length a as well as the out-of-plane tensile stress $\sigma(x)$ along the presupposed crack path (i.e. for $0 \le x \le a$, x is the distance to the free surface, Fig. 2) prior to fracture.

3. The coupled criterion

The coupled criterion states that crack onset occurs if two conditions are fulfilled simultaneously; the first one specifies that there is enough available energy to create a crack and the second that the tensile stress is greater than the tensile strength all along the presupposed new crack path:

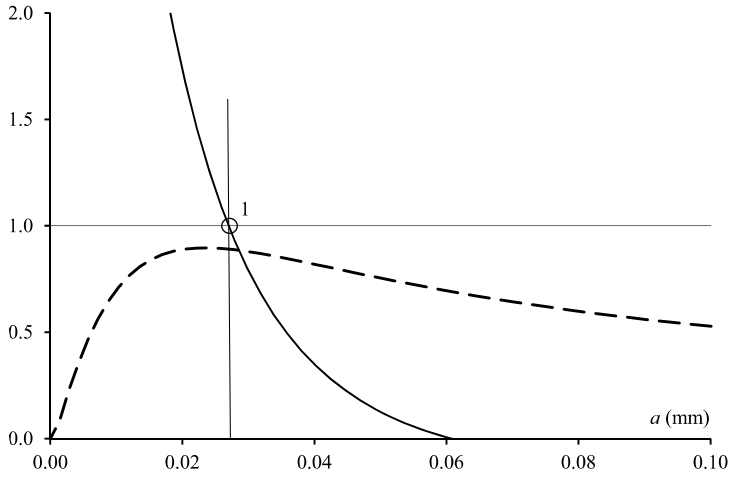

Fig. 3. The coupled criterion for $t_2 = 0.05$ mm and $\Delta\theta = -1000$ K. Energy condition: dashed line, stress condition: solid line (see Eq. (5)).

$$\begin{cases} -\delta W^{\mathrm{P}}(a) \geq G_{\mathrm{c}}^{(2)} a \\ \sigma(x) \geq \sigma_{\mathrm{c}}^{(2)} \quad \text{for } 0 \leq x \leq a \end{cases} \tag{2}$$

where $\delta W^{\mathrm{P}}(a)$ is the change in potential energy between the cracked and uncracked states and where $G_{\mathrm{c}}^{(2)}$ (MPa mm) and $\sigma_{\mathrm{c}}^{(2)}$ are respectively the toughness and the tensile strength of AMZ. The toughness $G_{\mathrm{c}}^{(2)}$ relies on $K_{\mathrm{Ic}}^{(2)}$ (Table 1) through the Irwin formula ($E^{(2)}$ and $\nu^{(2)}$ are the Young modulus and the Poisson ratio of AMZ):

$$G_{\mathrm{c}}^{(2)} = \frac{1-\nu^{(2)2}}{E^{(2)}} K_{\mathrm{Ic}}^{(2)2} = 0.023 \text{ MPa mm} \tag{3}$$

Using the incremental energy release rate $G^{\mathrm{inc}}(a)$ (MPa mm)

$$G^{\mathrm{inc}}(a) = -\delta W^{\mathrm{P}}(a)/a \tag{4}$$

and pointing out that $\sigma(x)$ is a decreasing function of x, (2) can be rewritten in a simple manner:

$$\frac{G^{\mathrm{inc}}(a)}{G_{\mathrm{c}}^{(2)}} \geq 1 \quad \text{and} \quad \frac{\sigma(a)}{\sigma_{\mathrm{c}}^{(2)}} \geq 1 \tag{5}$$

In this system of inequalities, the crack length a is up to now an unknown and there are two parameters, the intensity of the load, i.e. the temperature change $\Delta\theta$, and the AMZ layer thickness t_2.

4. Edge cracking

It is very convenient to plot the two conditions (5) in the same graph, as shown in Fig. 3. In the first case (Fig. 3, $t_2 = 0.05$ mm), the stress condition (solid line) holds for $a \leq 0.027$ mm (point 1), but the energy condition (dashed line) is nowhere fulfilled. Thus no edge cracking can appear. In the second case (Fig. 4, $t_2 = 0.07$ mm), the stress condition (solid line) holds for $a \leq 0.038$ mm (point 1) and the energy one (dashed line) for $0.014 \leq a \leq 0.079$ mm (points 2 and 3). Obviously, the two conditions are fulfilled in the range 0.014–0.038 mm (between points 1 and 2), and edge cracking can occur. Moreover, according to this coupled criterion, it is clear that the crack likely appears for a cooling amplitude $|\Delta\theta|$ smaller than 1000 K.

Note in these two figures that the tensile stress $\sigma(x)$ is very large, but drops rapidly away from the surface.

It is even possible to determine the cooling amplitude $|\Delta\theta|$ that causes edge cracking for different AMZ layer thicknesses. It decreases as the layer thickness increases (Fig. 5).

A comparison can be carried out with the formula proposed by Ho et al. [8] derived when neglecting the elastic mismatch between the two components (see [12]):

$$t_{\mathrm{c}}^{(2)} = \frac{K_{\mathrm{Ic}}^{(2)2}}{C\sigma_{\mathrm{R}}^{(2)2}} \quad \text{with } C = 0.34 \tag{6}$$

here $t_{\mathrm{c}}^{(2)}$ is the critical AMZ thickness above which edge cracking occurs for a given compressive residual stress $\sigma_{\mathrm{R}}^{(2)}$.

In the following table (Table 2), the constant C is recalculated using (6) for each AMZ layer thickness t_2 at crack initiation, keeping in mind that the ratio $2t_1/t_2$ remains constant. In this calculation, the residual stress $\sigma_{\mathrm{R}}^{(2)}$ depends on the cooling

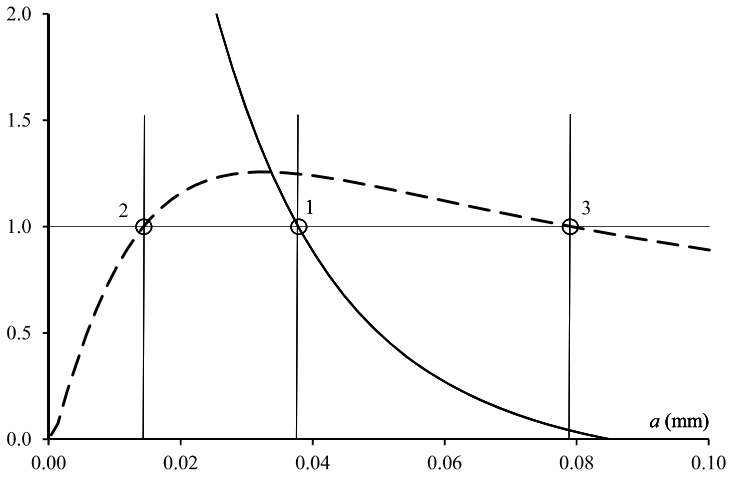

Fig. 4. The coupled criterion for $t_2 = 0.07$ mm and $\Delta\theta = -1000$ K. Energy condition: dashed line, stress condition: solid line (see Eq. (5)).

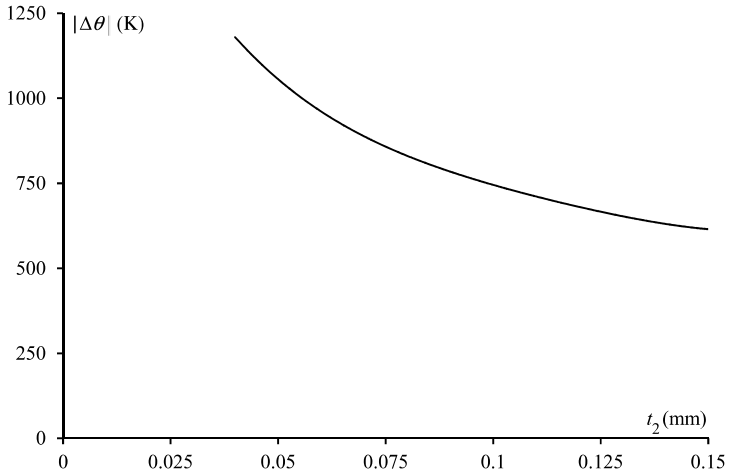

Fig. 5. The cooling amplitude $|\Delta\theta|$ that triggers edge cracking as a function of the AMZ layer thickness for a constant thickness ratio $2t_1/t_2 = 20$.

Table 2
Comparison with [8]. Here $|\Delta\theta|$ is the cooling amplitude that triggers cracking as a function of the AMZ layer thickness t_2 and $\sigma_R^{(2)}$ is the corresponding residual stress.

t_2 (mm)	$\lvert\Delta\theta\rvert$ (K)	$\sigma_R^{(2)}$ (MPa)	C
0.04	1180	−736	0.312
0.05	1055	−655	0.315
0.06	960	−599	0.314
0.07	890	−555	0.313
0.08	830	−518	0.315
0.09	785	−490	0.313
0.10	745	−465	0.313
0.11	710	−443	0.313
0.12	680	−424	0.313
0.13	655	−409	0.311
0.14	630	−393	0.312
0.15	615	−384	0.306

amplitude triggering the crack onset. A constant value emerges clearly, the resulting average is $\bar{C} = 0.31$, not far from the value proposed by Ho et al., but still slightly smaller. It means that the critical thickness predicted by the coupled criterion is a bit larger (+10%). This is qualitatively in agreement with a remark found in [12,17], but still below the experimental observations made there.

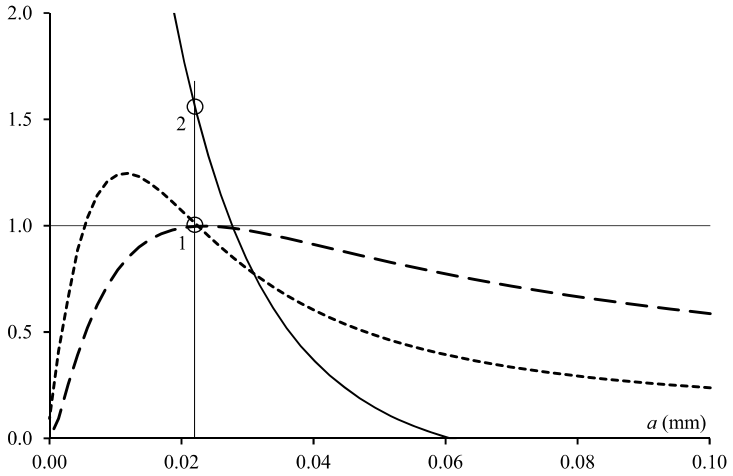

Fig. 6. The dimensionless incremental energy release rate $G^{\text{inc}}(a)/G_c^{(2)}$ (dashed line), the dimensionless energy release rate $G(a)/G_c^{(2)}$ (dotted line) and the dimensionless tensile stress $\sigma(a)/\sigma_c^{(2)}$ (solid line) for $t_2 = 0.05$ mm and $\Delta\theta = -1055$ K corresponding to the edge crack onset.

5. The growth of the edge crack

Once an edge crack is created, the further growth can be analyzed using the classical Griffith criterion based on the energy release rate $G(a)$ (MPa mm):

$$G(a) = -\frac{\partial W^{\text{P}}(a)}{\partial a} \tag{7}$$

According to Griffith, crack growth occurs if $G(a) \geq G_c^{(2)}$.

The dimensionless energy release rate $G(a)/G_c^{(2)}$ is plotted in Fig. 6 (dotted line) for $t_2 = 0.05$ mm and $\Delta\theta = 1055$ K, corresponding to the edge crack onset. The two conditions (5) hold true at a single point $a = 0.023$ mm (point 1). Moreover, it is clear that the crack onset is mainly governed by the energy condition since at this point the stress condition is well above the threshold (point 2).

At point $a = 0.023$ mm, $G(a) = G_c^{(2)}$ and $G(a)$ is a decreasing function of the crack length a (it can be shown that if $\partial G^{\text{inc}}(a)/\partial a = 0$ at a point then $G(a) = G^{\text{inc}}(a)$ at this point); as a consequence, the point under consideration is an arrest point.

If cooling is going on with an increasing temperature amplitude, the curves are shifted upward (Fig. 7). The first one corresponds to the crack onset $\Delta\theta = -1055$ K and a crack length $a = 0.023$ mm, as already mentioned. The next one is for $\Delta\theta = -1300$ K and it is clear that, between the two states, crack growth is stable and follows the temperature change, now $a = 0.037$ mm. Even for an unrealistic temperature change, as $\Delta\theta = -1500$ K, the crack growth is still stable and the crack length reaches the value $a = 0.048$ mm. Clearly, an edge cracking cannot lead to a complete ruin of the specimen under realistic thermal loads.

Other calculations have been carried out with $t_1 = 0.54$ mm, $t_2 = 0.095$ mm and $t_1 = 0.57$ mm, $t_2 = 0.06$ mm corresponding to the stacking sequences B and C in [10,12] but with the simplified geometry of Fig. 1. Edge cracking is predicted to occur for $\Delta\theta_{\text{B}} = -790$ K and $\Delta\theta_{\text{C}} = -965$ K respectively. There is a wide gap in temperature showing that edge cracking occurs much earlier in structure B than in structure C. This is qualitatively in agreement with the observations reported in [12], for the same thermal treatment structure B exhibits an edge crack while structure C does not. Nevertheless, in [12] the corresponding theoretical temperature drop is $\Delta\theta \approx -1180$ K (derived from the thermal strain mismatch $\Delta\varepsilon = (\alpha^{(2)} - \alpha^{(1)})\Delta\theta$ reported to be $\Delta\varepsilon = 2.12 \cdot 10^{-3}$), leading to higher residual stresses than predicted here. It does not seem possible to invoke the present simplified geometry to explain the discrepancy. Indeed, the same stress levels are reached in the present geometry for $\Delta\theta_{\text{B}} = -1137$ K and $\Delta\theta_{\text{C}} = -1153$ K respectively, not so far from -1180 K. But the exact residual stress state in the laminate is difficult to determine precisely. There is no direct measure and numerical results are based on the assumption of a stress-free state around 1200 °C. The indentation tests made on the ATZ layers [10] show that the FE calculations tend to overestimate the stress values based on this hypothesis.

Note that the predictions are again mainly governed by the energy condition (Fig. 6) and they are sensitive to the measured value of the toughness. If $K_{\text{Ic}}^{(2)}$ is increased by 10%, then according to Table 1 and (3), $G_c^{(2)} = 0.028$ MPa · mm and the temperature changes leading to cracking are shifted toward $\Delta\theta_{\text{B}} = -870$ K and $\Delta\theta_{\text{C}} = -1065$ K.

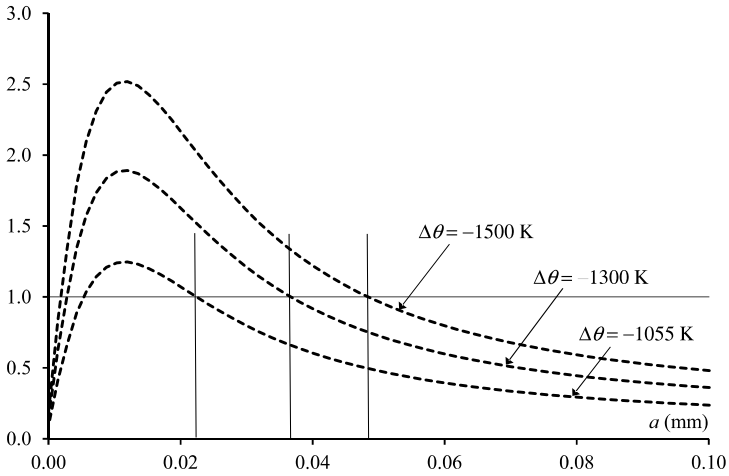

Fig. 7. The dimensionless energy release rate $G(a)/G_c^{(2)}$ for different cooling amplitudes.

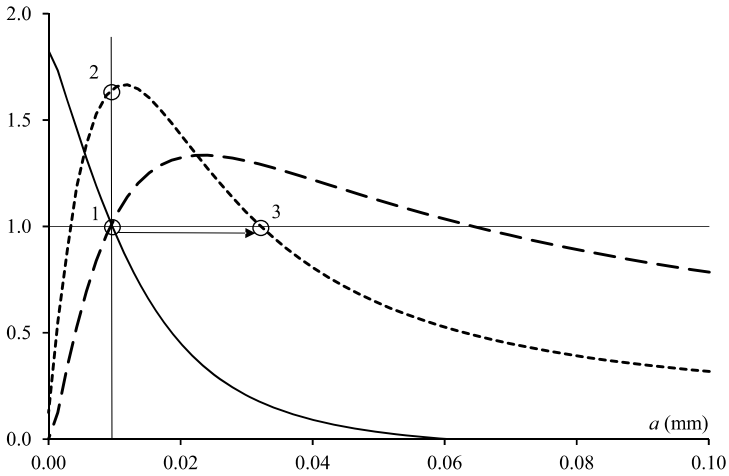

Fig. 8. The dimensionless incremental energy release rate $G^{\text{inc}}(a)/G_c^{(2)}$ (dashed line), the dimensionless energy release rate $G(a)/G_c^{(2)}$ (dotted line), and the dimensionless tensile stress $\sigma(a)/\sigma_c^{(2)}$ (solid line) for $t_2 = 0.05$ mm and $\Delta\theta = -1220$ K, corresponding to the edge crack onset.

6. Energy-governed and stress-governed edge cracking

The title of this section may seem ambiguous for a criterion where the two conditions in energy and stress are necessary. The distinction between the two concepts is based on the question of which of these two conditions is reached first in a monotonic thermal loading, the other one becoming predominant in order to fulfill the criterion. In Fig. 6, it is clear that the stress condition is fulfilled first and that the final load level is mainly determined by the energy condition, this is why it is called energy-governed cracking. Instead, we will see in the example below that the energy condition is reached first and that the thermal load must continue to increase to meet the stress condition. We are in the presence of the so-called stress-governed cracking.

Let us consider again the case illustrated in Fig. 6 and suppose, for the aim of the discussion, that the tensile strength of AMZ is higher than its current value: $\sigma_c^{(2)} = 422$ MPa (the tensile strength of ATZ). The solid line representing the dimensionless tensile stress is moved to the left far beyond point 1 in Fig. 6, while the dashed line, the dimensionless incremental energy release rate, is unchanged. Thus, there is no longer any point fulfilling the two conditions (5), edge cracking cannot occur for $\Delta\theta = -1055$ K and the thermal load must be increased, i.e. cooling must go on, for finding a new solution (Fig. 8). This is achieved for $\Delta\theta = -1220$ K and $a = 0.01$ mm (point 1). The situation (Fig. 8) is now different from the previous one (Fig. 6). At point $a = 0.01$ mm, the energy release rate (dotted line) is strictly greater than the material's toughness $G(a) > G_c^{(2)}$ (point 2) and the crack grows (arrow) in an unstable manner up to point 3 ($a = 0.032$ mm), where $G(a)$ drops below $G_c^{(2)}$. Point 3 is the first possible arrest point, but the crack can even grow a little bit further if part or all of the additional energy generated between points 1 and 3 (where $G(a) > G_c^{(2)}$) is consumed by fracture. Again the crack does not extend far in depth except for considering an unrealistically large cooling.

7. Conclusion

The 2D coupled criterion is quite simple to use and has proved to be rather effective in the prediction of edge cracking in ceramic laminates. But it is clear that a more striking confirmation of the model would require knowing better the state of residual stresses in the sample after heat treatment. The present prediction is achieved with very little information: the elastic moduli of the layers, their coefficient of thermal expansion, the toughness and the tensile strength of the compressive layer. There is no adjustable parameter and there is no need for an assumption on the presence of surface defects to initiate fracture. This may seem surprising, but if the presence of a major flaw far larger than the others is excluded – this case should be treated separately –, it must be pointed out that the values of the material's parameters used in the analysis are of course homogenized. Their measure takes into account a population of distributed micro-defects; thus the presence of flaws is not totally absent from this analysis, but averaged somewhat, like $E^{(2)}$, $K_{\mathrm{Ic}}^{(2)}$ and $\sigma_{\mathrm{c}}^{(2)}$ are.

Acknowledgement

Oldrich Sevecek gratefully acknowledges a financial support through the project CZ.1.07/2.3.00/30.0005 of Brno University of Technology.

References

[1] A.G. Evans, Perspective on the development of high-toughness ceramics, J. Am. Ceram. Soc. 73 (1990) 187–206.
[2] A.J. Phillipps, W.J. Clegg, T.W. Clyne, The failure of layered ceramics in bending and tension, Composites 25 (1994) 524–533.
[3] R.J. Kerans, R.S. Hay, T.A. Parthasarathy, M.K. Cinilbulk, Interface design for oxidation-resistant ceramic composite, J. Am. Ceram. Soc. 85 (2002) 2599–2632.
[4] R. Naslain, Design, preparation and properties of non-oxide CMCs for application in engines and nuclear reactors: an overview, Compos. Sci. Technol. 64 (2004) 155–170.
[5] K.S. Blanks, A. Kristofferson, E. Carlström, W.J. Clegg, Crack deflection in ceramic laminates using porous interlayers, J. Eur. Ceram. Soc. 18 (1998) 1945–1951.
[6] J.B. Davis, A. Kristoffersson, E. Carlström, W.J. Clegg, Fabrication and crack deflection in ceramic laminates with porous interlayers, J. Am. Ceram. Soc. 83 (2000) 2369–2374.
[7] C. Reynaud, F. Thevenot, T. Chartier, J.-L. Besson, Mechanical properties and mechanical behaviour of SiC dense-porous laminates, J. Eur. Ceram. Soc. 25 (2005) 589–597.
[8] S. Ho, C. Hillman, F.F. Lange, Z. Suo, Surface cracking in layers under biaxial residual compressive stress, J. Am. Ceram. Soc. 85 (1995) 1222–1228.
[9] A. Atkinson, A. Selçuk, Residual stress and fracture of laminated ceramic membranes, Acta Mater. 47 (1999) 867–874.
[10] R. Bermejo, Y. Torres, A.J. Sanchez-Herencia, C. Baudin, M. Anglada, L. Llanes, Residual stresses, strength and toughness of laminates with different layer thickness ratios, Acta Mater. 54 (2006) 4745–4757.
[11] R. Bermejo, J. Pascual, T. Lube, R. Danzer, Optimal strength and toughness of Al_2O_3/ZrO_2 laminates designed with external or internal compressive layers, J. Eur. Ceram. Soc. 28 (2008) 1575–1583.
[12] C.R. Chen, R. Bermejo, O. Kolednik, Numerical analysis on special cracking phenomena of residual compressive inter-layers in ceramic laminates, Eng. Fract. Mech. 77 (2010) 2567–2576.
[13] D. Leguillon, Strength or toughness? A criterion for crack onset at a notch, Eur. J. Mech. A, Solids 21 (2002) 61–72.
[14] E. Martin, D. Leguillon, Energetic conditions for interfacial failure in the vicinity of a matrix crack in brittle matrix composites, Int. J. Solids Struct. 41 (2004) 6937–6948.
[15] O. Sevecek, R. Bermejo, M. Kotoul, Prediction of the crack bifurcation in layered ceramics with high residual stresses, Eng. Fract. Mech. 108 (2013) 120–138.
[16] D. Leguillon, O. Haddad, M. Adamowska, P. Da Costa, Cracks pattern formation and spalling in functionalized thin films, Procedia Mater. Sci. 3 (2014) 104–109.
[17] M.P. Rao, F.F. Lange, Factors affecting threshold strength in laminar ceramics containing thin compressive layers, J. Am. Ceram. Soc. 85 (2002) 1222–1228.